Supporting Information for

High-Capacity Electrode Materials for Rechargeable Lithium Batteries: Li_3NbO_4-based System with Cation Disordered Rocksalt Structure

Naoaki Yabuuchi[1]*, Mitsue Takeuchi[2], Masanobu Nakayama[3,4], Hiromasa Shiiba[3], Masahiro Ogawa[5], Keisuke Nakayama[5], Toshiaki Ohta[5], Daisuke Endo[6], Tetsuya Ozaki[6], Tokuo Inamasu[6], Kei Sato[1], and Shinichi Komaba[2]*

1) Department of Green and Sustainable Chemistry, Tokyo Denki University

5 Senju Asahi-Cho, Adachi, Tokyo 120-8551, Japan

2) Department of Applied Chemistry, Tokyo University of Science,

1-3 Kagurazaka, Shinjuku, Tokyo 162-8601, Japan

3) Department of Materials Science and Engineering, Nagoya Institute of Technology,

Gokiso-cho, Showa-ku, Nagoya, Aichi 466-8555, Japan

4) Japan Science and Technology Agency (JST), PRESTO, 4-1-8 Honcho Kawaguchi, Saitama 332-0012, Japan

5) SR Center, Ritsumeikan University, 1-1-1 Noji-Higashi, Kusatsu, Shiga 525-8577, Japan

6) R&D Center, GS Yuasa International Ltd., Minami-ku, Kyoto 601-8520, Japan

*co-corresponding author: yabuuchi@mail.dendai.ac.jp, komaba@rs.kagu.tus.ac.jp

Methodology for DFT calculation

Ab initio calculations based on density functional theory (DFT) for Li_3NbO_4–$LiMnO_2$ system were performed using Vienna ab initio simulation package (VASP)(1, 2) with modified Perdew-Burke-Ernzerhof generalized gradient approximation (PBEsol-GGA)(3, 4) and with the projector-augmented wave (PAW) method.(5) Besides, the on-site Coulomb correction (GGA + *U*) was included for localized electronic states, and *U* value was chosen to be 3.9 eV for Mn 3*d* states and 1.5 eV for Nb 3*d* states, according to the literature.(6)

In the present calculations, the molar ratio of Nb and Mn was set as 1:1, *i.e.* $Li_{4/3}Nb_{1/3}Mn_{1/3}O_2$, for convenience sake, unless specially mentioned in the manuscript. The most stable cationic arrangement for Li, Nb and Mn ions in $Li_{4/3}Mn_{1/3}Nb_{1/3}O_2$ with rocksalt-related structures was determined among 206 candidates.

References

1 Kresse, G. & Furthmuller, J. Efficient iterative schemes for ab initio total-energy calculations using a plane-wave basis set. *Physical Review B* **54**, 11169-11186, doi:10.1103/PhysRevB.54.11169 (1996).

2 Kresse, G. & Furthmuller, J. Efficiency of ab-initio total energy calculations for metals and semiconductors using a plane-wave basis set. *Computational Materials Science* **6**, 15-50, doi:10.1016/0927-0256(96)00008-0 (1996).

3 Perdew, J. P., Burke, K. & Ernzerhof, M. Generalized gradient approximation made simple. *Physical Review Letters* **77**, 3865-3868, doi:10.1103/PhysRevLett.77.3865 (1996).

4 Perdew, J. P. *et al.* Restoring the density-gradient expansion for exchange in solids and surfaces. *Physical Review Letters* **100**, doi:10.1103/PhysRevLett.100.136406 (2008).

5 Blochl, P. E. PROJECTOR AUGMENTED-WAVE METHOD. *Physical Review B* **50**, 17953-17979, doi:10.1103/PhysRevB.50.17953 (1994).

6 Hautier, G., Ong, S. P., Jain, A., Moore, C. J. & Ceder, G. Accuracy of density functional theory in predicting formation energies of ternary oxides from binary oxides and its implication on phase stability. *Physical Review B* **85**, doi:10.1103/PhysRevB.85.155208 (2012).

Table S1. Calculated net-moment of transition metals versus composition y in $Li_{(4-y)/3}Nb_{1/3}Mn_{1/3}O_2$. The net-moment is defined as the amount of electron spin up minus the electron spin down at the integration radius (1.4 Å) around both Nb and Mn ion cores.

Composition y	0	1	2	3	4
Nb	+0.02	+0.02	+0.04	+0.06	+0.002
Mn	+3.87	+3.34	+3.17	+3.13	+0.03

Remarks on Table S1;

The variation of oxidation state of cations and anions in $Li_{(4-y)/3}Mn_{1/3}Nb_{1/3}O_2$ was evaluated by net-spin moments around transition ions as listed in Supporting **Table S1**. The net-spin moments of Nb ions are ~ 0 for all the composition range, in which the oxidation state of Nb ions corresponds to +5 with the d^0 electronic configuration. Therefore, Nb ions are considered to be electrochemically inactive as the redox species during electrochemical charge/discharge process. (This result also agrees with the variation of Nb XAS spectra shown in **Figure S6**) Net-spin moments of Mn ions indicate the oxidation from Mn^{3+} (t_{2g}^3 e_g^1) to Mn^{4+} (t_{2g}^3) at the initial charge process ($0 \leq y \leq 1$). However, no marked change was indicated in the net-moments of Mn ions for further delithiation from y = 1 to 3 even though the nominal valence state of Mn ions is expected to change from +4 to +6 based on the solid-state redox of manganese ions. Thus, the results indicate oxide ions contribute to charge compensation for the charge/discharge reaction in the composition range, $1 \leq y \leq 3$. Net-moments of Mn ions are then reduced to ~ 0 for the completely delithiated phase of $Nb_{1/3}Mn_{1/3}O_2$ (y = 4). This result may be due to the change of electronic configuration of Mn ions from Mn^{4+} to Mn^{7+} with d^0 configuration through the DOS analyses in **Figure 3c**.

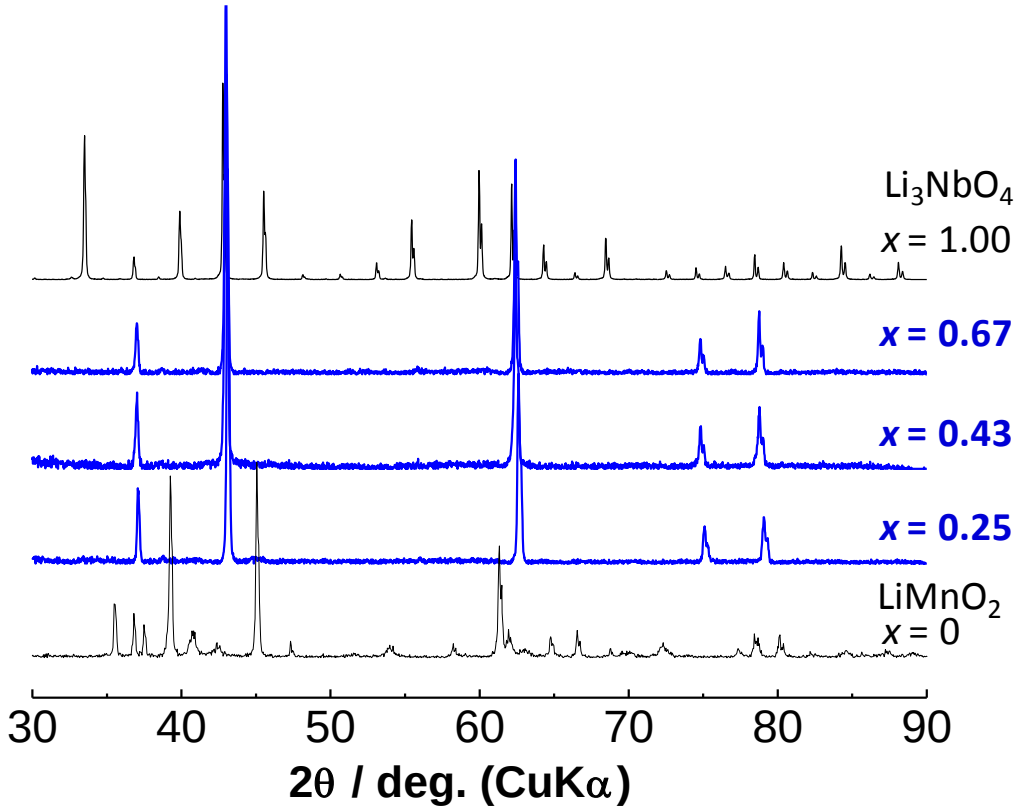

Figure S1. XRD patterns of a binary system between two different cation-ordered rocksalt superstructures, Li_3NbO_4 and $LiMnO_2$: Cation-disordered rocksalt phase is obtained in the range of $0.25 \leq x \leq 0.67$ in xLi_3NbO_4–$(1-x)LiMnO_2$. A crystal structure of $LiMnO_2$ without niobium ions is assigned as an orthorhombic lattice with a space group of *Pmm*2. Clustering of niobium ions is disturbed in this binary system, forming the cation-disordered rocksalt structure.

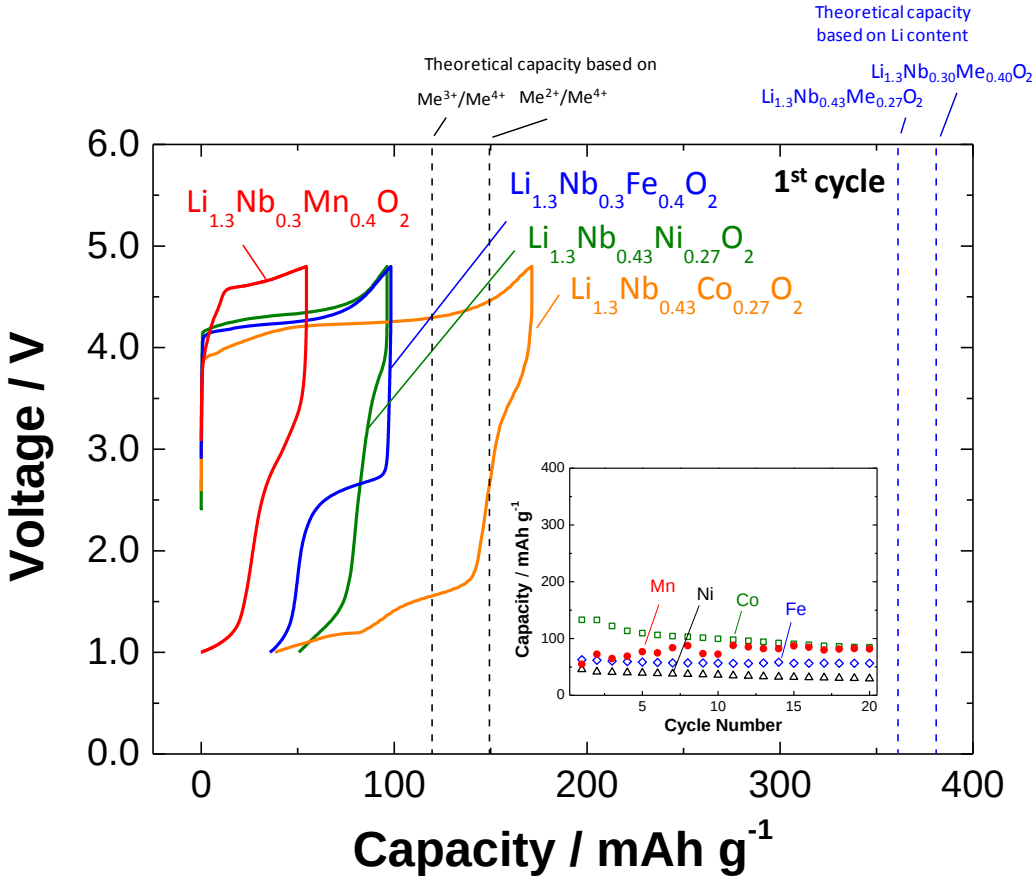

Theoretical capacity

Samples	based on **Li⁺** (mAh g^{-1})	**redox of TMs** (mAh g^{-1})
$Li_{1.3}Nb_{0.43}Me^{2+}_{0.27}O_2$	**360**	**150 ($Me^{2+/4+}$)**
$Li_{1.3}Nb_{0.30}Me^{3+}_{0.40}O_2$	**380**	**118 ($Me^{3+/4+}$)**

Figure S2. Charge/discharge curves of as-prepared Li_3NbO_4-based electrode materials in Li cells at a rate of 10 mA g^{-1} at room temperature. The composite electrodes used consisted of active material : AB : PVDF = 80 : 10 : 10 (wt %). Theoretical capacities based on the redox reaction of transition metals and based on the contents of Li ions in the samples are also shown. Reversible capacities observed for the as-prepared samples show good agreement with the theoretical capacities based on the redox of only transition metals. Capacity retention of the samples is also shown in the inset.

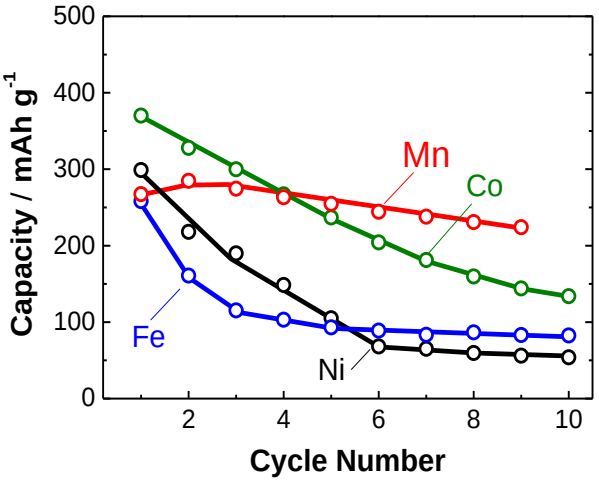

Figure S3. Capacity retention of the ballmilled Li_3NbO_4-based electrode materials at a rate of 10 mA g^{-1} in the voltage range of 1.0 and 4.8 V at room temperature. Charge/discharge curves of the Li cells are found in **Figure 2**.

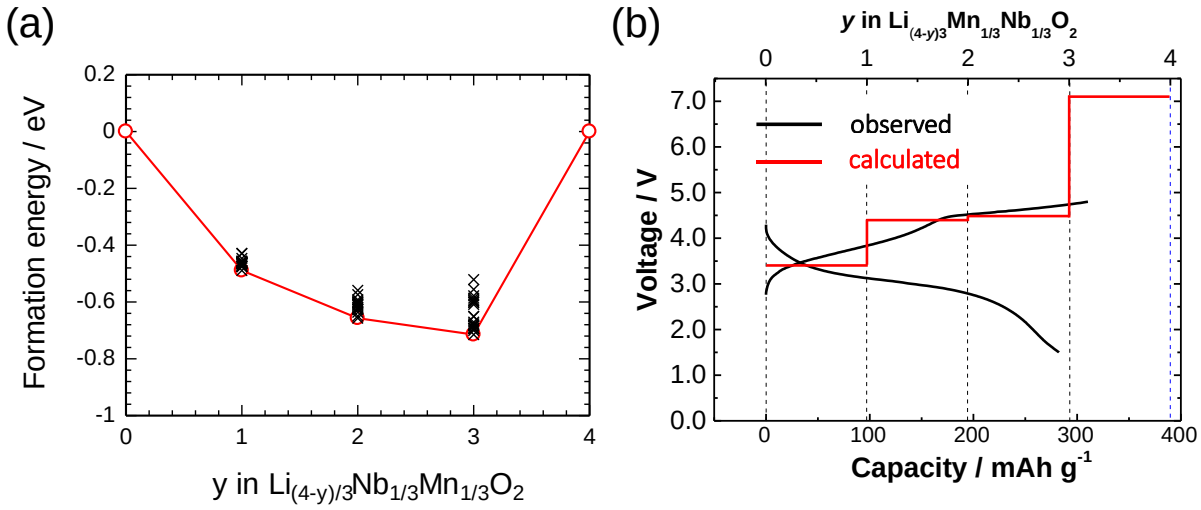

Figure S4. Phase stability with electrochemical charging in $L_{(4-y)/3}Mn_{1/3}Nb_{1/3}O_2$ as calculated with the DFT method: (a) Formation energies with various Li^+/vacancy configurations are plotted as a function of composition *y*. The convex hull is drawn connecting the structures with the lowest formation energies. (b) Red line indicates calculated voltage profile using the convex hull, and is in good agreement with present experimental one. The calculated voltage profile agrees well with experimental one in the compositional range from $y = 0$ to 3. The voltage exceeds 7.0 V at $y = 3$ to 4, due to the instability of $Nb_{1/3}Mn_{1/3}O_2$ phase, and thus it also agrees with the fact that experimental reversible capacity was limited to less than 300 mAh g^{-1} (**Figure 2d**).

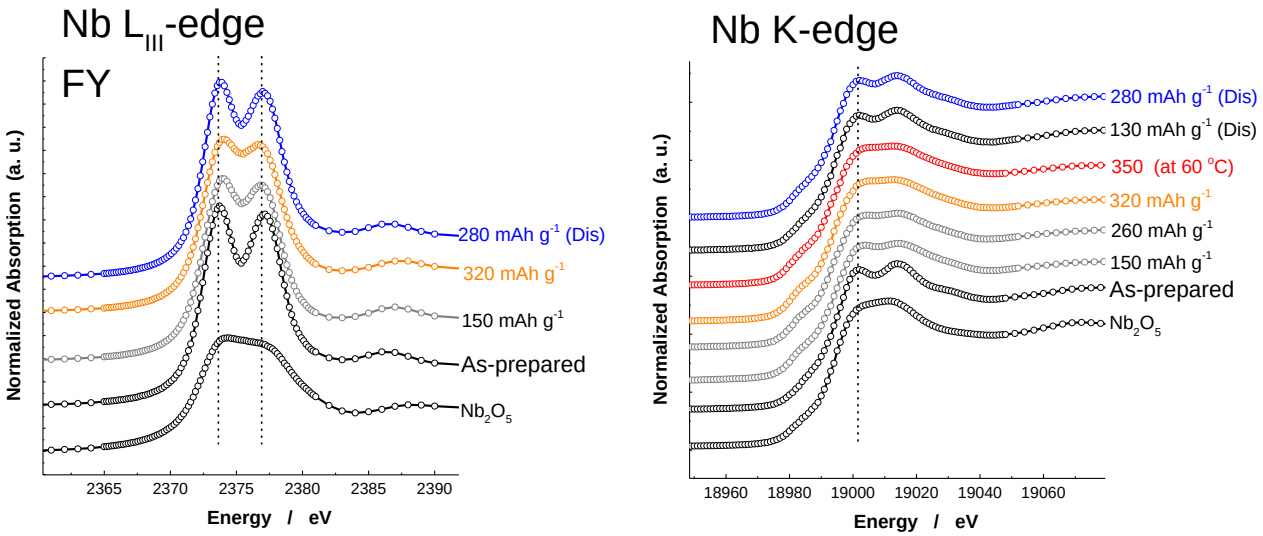

Figure S5. Nb L_{III}-edge and Nb K-edge absorption spectra, collected for the charged/discharged samples. No change in the peak position is observed even after discharge. Nb oxidation state is found to be not affected by charge/discharge process even though peak profile is slightly changed by charge process. This fact shows that niobium ions are stabilized at pentavalent state and are not reduced by discharge, indicating that niobium ions are not responsible for the large discharge capacity of $Li_{1.3}Nb_{0.3}Mn_{0.4}O_2$ as the redox center.

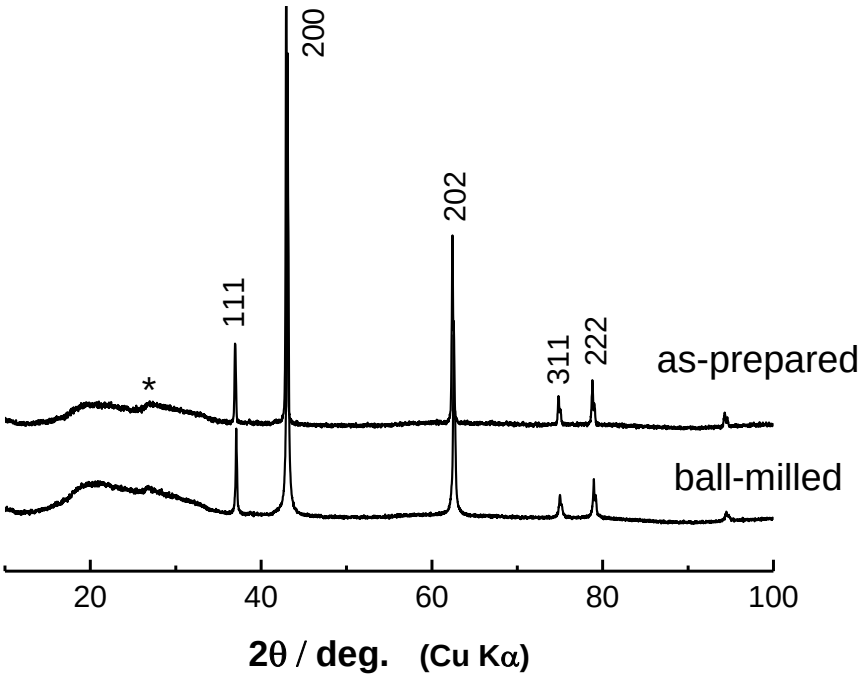

Figure S6. X-ray diffraction patterns of the modified $Li_{1.3}Nb_{0.3}Mn_{0.4}O_2$; before and after ball-milling. No

impurity phase is found. A lattice parameter of the ball-milled sample was calculated to be a = 4.19 Å. The small peak denoted by an asterisk originates from the airtight sample holder.

Remarks on Figures S6;

The modified $Li_{1.3}Nb_{0.3}Mn_{0.4}O_2$ was synthesized from Mn_2O_3, Nb_2O_5, and Li_2CO_3 by solid-state reaction. The precursors were thoroughly mixed by wet mechanical ball-milling and then dried in air. Thus obtained mixture of the samples was pressed into a pellet. The pellet was heated at 900 ^oC for 6 h in Ar, which is lower temperature and shorter time than those used for synthesis of the original sample. Thus obtained sample was mixed with 10 wt% acetylene black (HS-100, Denki Kagaku Kogyo, Co. Ltd., Japan) by ball-milling. To prepare the slurry, 85 wt% carbon composite sample ($Li_{1.3}Nb_{0.3}Mn_{0.4}O_2$: AB = 9 : 1 in a weight ratio) was mixed using a mortar and pestle with additional 5 wt% acetylene black and 10 wt% poly(vinylidene fluoride), and pasted on aluminium foil as a current collector. The total carbon content in the composite electrode is also reduced to 13.5 wt% (18 wt% in the composite electrodes used in **Figures 2 – 4**). Particle morphology is shown in **Supporting Figure S6**.

The Original Sample Used in Figures 2 and 4

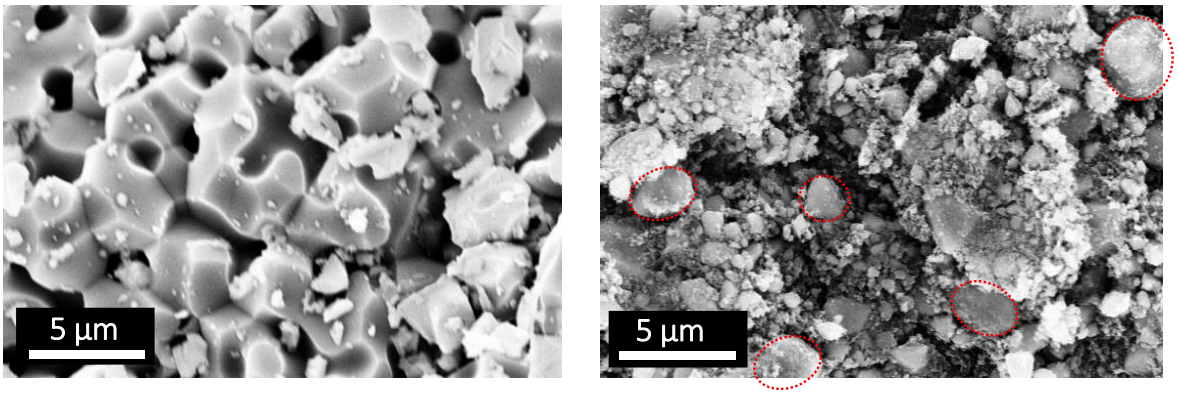

As-prepared

Ball-milled
(80 wt% sample + 20 wt% A.B.)

The Modified Sample Used in Figure 5

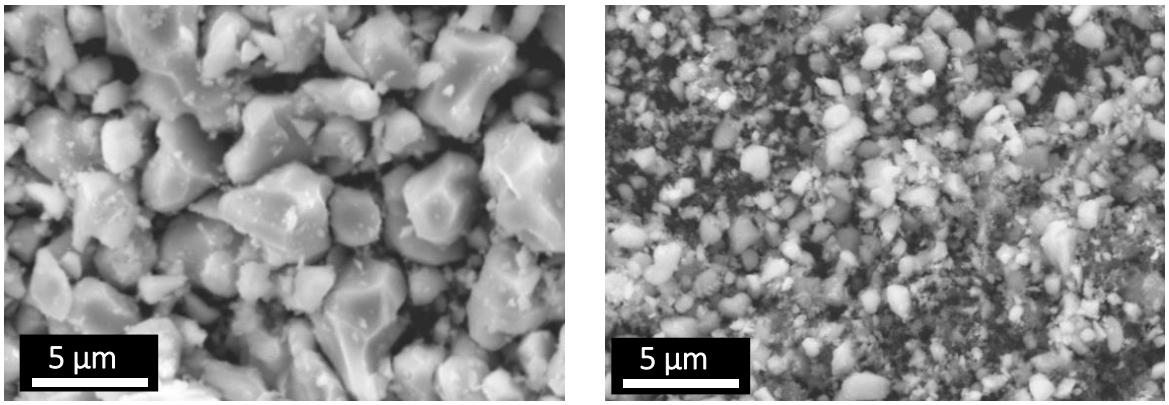

As-prepared

Ball-milled
(90 wt% sample + 10 wt% A.B.)

Figure S7. Particle morphology of different $Li_{1.3}Nb_{0.3}Mn_{0.4}O_2$ samples observed by SEM; as-prepared and ball-milled samples with acetylene black. After ball-milling, $Li_{1.3}Nb_{0.3}Mn_{0.4}O_2$ powders and nano-sized carbon materials are non-uniformly mixed in the original sample, and relatively large $Li_{1.3}Nb_{0.3}Mn_{0.4}O_2$ particles (marked by dotted red circles) are still present. In contrast, powders with uniform size and morphology are found in the modified sample. The morphological features of the samples were observed using a scanning electron microscope (Carl Zeiss, SUPRA40).

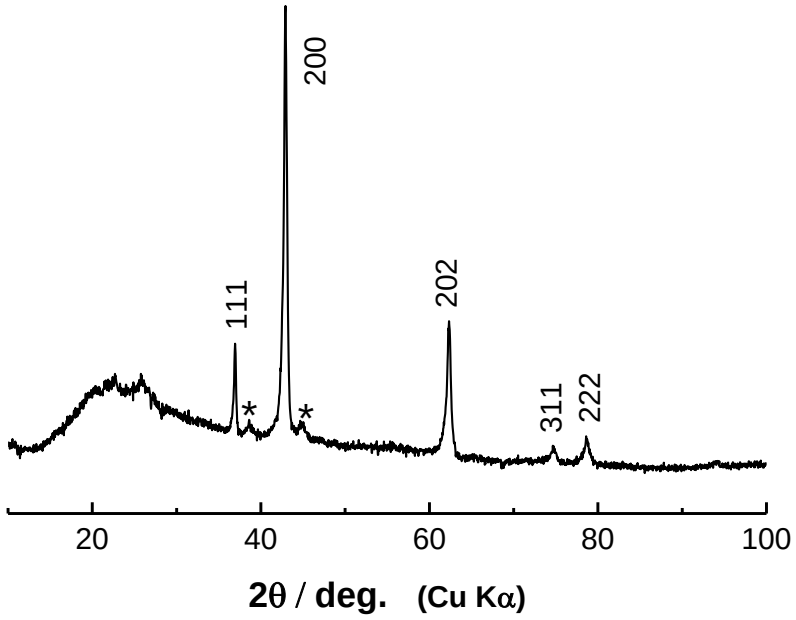

Figure S8. The XRD pattern of the electrode after 20-cycle test by charge with constant capacity of 250 mAh g^{-1}. Charge/discharge curves are shown in **Figure 5d and e**. Asterisks denote peaks from aluminum metal residue used as current collector.

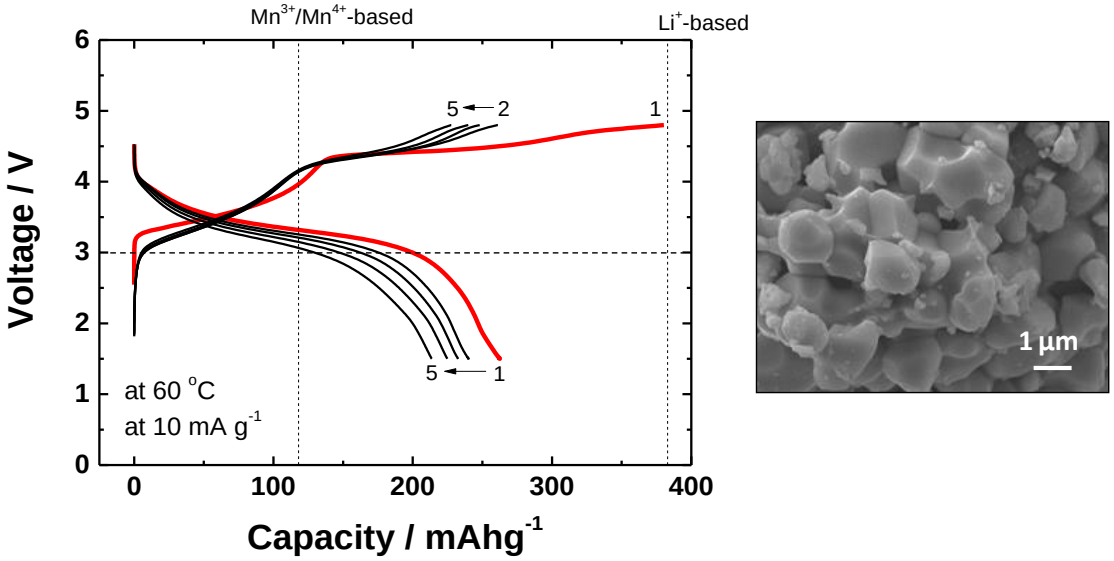

Figure S9. Electrode performance and particle morphology of $Li_{1.3}Nb_{0.3}Mn_{0.4}O_2$ prepared with the different synthesis condition. The sample is used as the electrode material without the ballmilling treatment with carbon. Composite electrode consisted of 80 wt% sample, 10 wt% acetylene black, and 10 wt% PVdF, which is the same experimental condition with the samples used in **Supporting Figure S2**. The electrochemical cell was cycled at 60 °C at a rate of 10 mA g^{-1} in the voltage range of 1.5 and 4.8 V.